Applied Catalysis B: Environmental 338 (2023) 122931

Contents lists available at ScienceDirect

Applied Catalysis B: Environmental

journal homepage: www.elsevier.com/locate/apcatb

Self-driven electron enrichment of ultrafine PdAu nanoparticles for electrochemical CO_2 reduction: High applicability of work function as an activity descriptor

Fengshou Yu [a], Guomeng Liu [a], Jiayu Zhan [a], Yangting Jia [a], Zhihao Feng [a], Boxiong Shen [a,*], N. Raveendran Shiju [b,*], Lu-Hua Zhang [a,*]

[a] Hebei Provincial Key Laboratory of Green Chemical Technology and High Efficient Energy Saving, Tianjin Key Laboratory of Chemical Process Safety, School of Chemical Engineering and Technology, Hebei University of Technology, Tianjin 300130, PR China
[b] Van 't Hoff Institute for Molecular Sciences, University of Amsterdam, P.O. Box 94157, 1090GD Amsterdam, the Netherlands

ARTICLE INFO

Keywords:
Electrochemical CO_2 reduction
Work function
Electron enrichment
Heterostructure

ABSTRACT

Highly coupled metal/dopant-incorporated carbon dyads provide a possibility to modulate the electron density of metallic materials by forming a rectifying interface, thus showing an enhanced activity in electrochemical CO_2 reduction reaction (ECRR). However, understanding the promotion effects of dopants for ECRR is limited to the prediction by theoretical interpretation and case-by-case studies. Herein, we report the direct experimental evidence that the work function, regulated by single structural factor-dopant contents, is significantly correlated to the ECRR reaction activity and kinetics. We prepared a series of PdAu/N_xC electrocatalysts composed of ultrafine (~5.7 nm) PdAu bimetallic nanoparticles and tailorable N-doped carbon supports. The wide range of the amount of N dopants allowed the modification of the band gap of the carbon easily. Using ultraviolet photoelectron spectroscopy (UPS) measurements, we demonstrate that the reactivity and kinetics trends of the PdAu/N_xC in the ECRR can be intrinsically correlated with the work function of the catalysts. PdAu/$N_{7.50}C$ electrocatalyst with the highest N contents displays a 100% CO_2-to-CO conversion and high conversion efficiency over a wide potential window, superior over other reported PdAu catalysts. This work provides a novel way to boost ECRR performance by deliberately lowering the work function of the metal/carbon electrocatalysts through the enhancement by dopants.

1. Introduction

Electrochemical CO_2 reduction reaction (ECRR) is an effective way to realize the utilization and conversion of CO_2 into highly value-added chemicals.[1–4] To facilitate this sluggish kinetics process, pioneering works of electrocatalyst design have demonstrated a size dependent ECRR performance on metallic electrocatalysts. The small-sized nanoparticles (NPs) usually show high catalytic activity, while they tend to agglomerate in a non-controlled manner during electrocatalytic reactions.[5–9] To avoid the agglomeration, arrangement of the NPs in/on porous carbon supports and simultaneous/further doping of heteroatoms into carbon lattice has been considered a good strategy to enhance the stability.[10–13] More importantly, the introduction of heteroatoms enlarges the band gap of carbon support, giving it a character of semiconductor materials, by which the interface potential was formed due to the different work function between metal and dopant-incorporated carbon support.[14–16] The difference in work function can drive the flow of electrons across the metal/carbon interfaces until heterojunctions reach the thermodynamic equilibrium state.[17–19] As a result, the heterojunction is highly capable of regulating the electron density of metal NPs.

Recent studies have demonstrated that the more electrons of the metal component is accepted or donated from the carbon support, the higher catalytic performance can be achieved.[20,21] In this regard, the work function can be a descriptor for catalytic performance, while these suggestions are based mainly on theoretical interpretation.[22] Some experimental studies showed a positive correlation between the catalytic activity and the work function for the supported nano catalysts.[23,24] However, the case-by-case studies based on two or three samples lack systematic theoretical and experimental explorations. The major

* Corresponding authors.
E-mail addresses: shenbx@hebut.edu.cn (B. Shen), n.r.shiju@uva.nl (N.R. Shiju), luhuazhang@hebut.edu.cn (L.-H. Zhang).

https://doi.org/10.1016/j.apcatb.2023.122931
Received 4 January 2023; Received in revised form 25 May 2023; Accepted 28 May 2023
Available online 5 June 2023

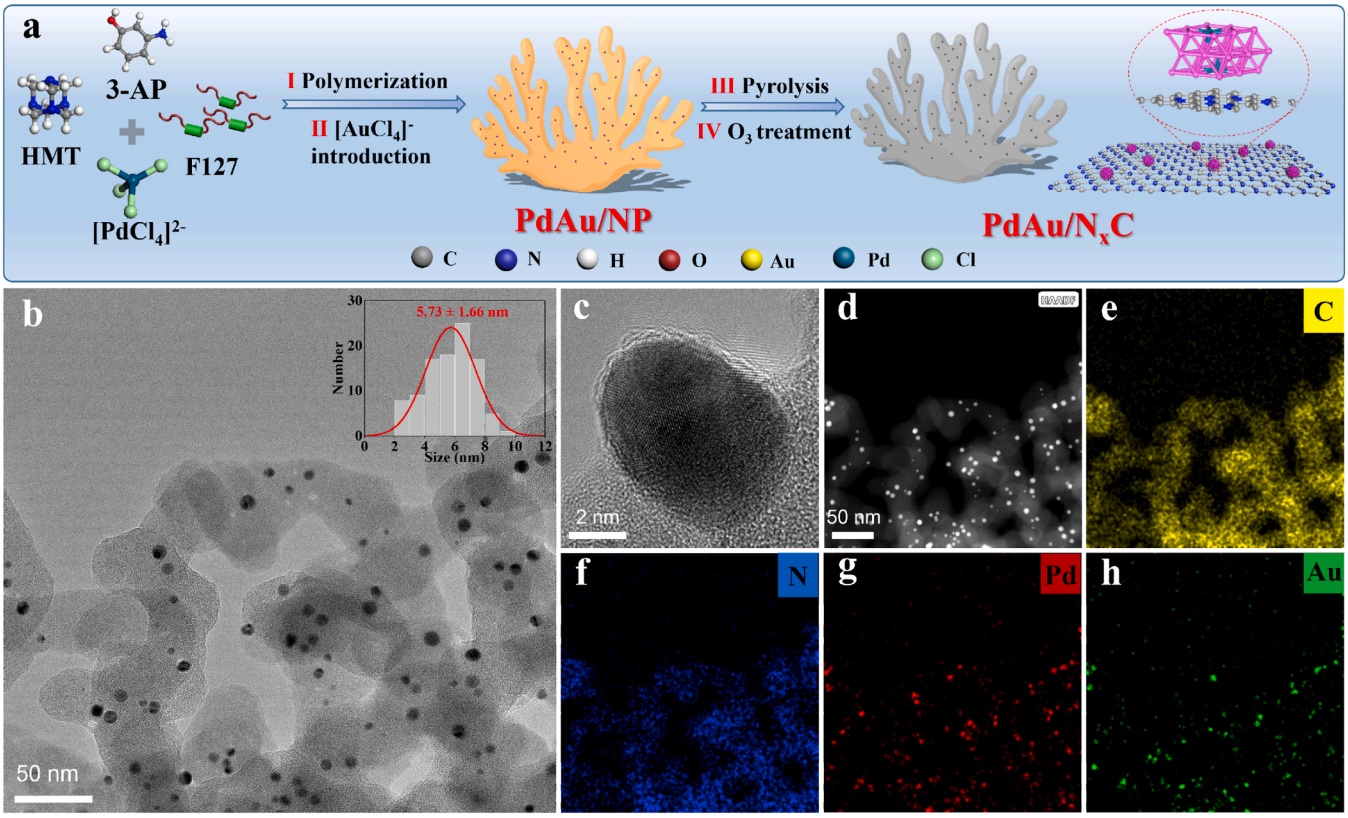

Fig. 1. (a) Procedure for PdAu/N_xC synthesis, (b) TEM image and the corresponding particle size distribution (inset) of PdAu/N_xC, (c) high-resolution TEM image, (d) STEM image and (e-h) the corresponding elemental mappings of PdAu/$N_{7.50}$C sample.

obstacle lies in that the interfacial electron transfer is affected by many factors, such as the type of dopants, the content of metal, and size of metal NPs. Also, there are marked interactions among various factors. [25–28] Systematic experimental correlation of a specific factor affecting the interface electron transfer in metal/carbon dyads with ECRR performance is rarely reported, yet it is critical for the design of metal/carbon composite electrocatalysts.

Herein, we report the direct experimental evidence that the work function, regulated by single structural factor-dopant contents, is significantly correlated to the ECRR reaction activity and kinetics. We prepared a series of PdAu/N_xC electrocatalysts composed of ultrafine (~5.7 nm) PdAu bimetallic NPs and tailorable N-doped carbon supports for ECRR. The wide range of the amount of N dopants allowed the modification of the band gap of the carbon easily, where more N creates a higher degree of charge separation in the interface. Using the ultraviolet photoelectron spectroscopy (UPS) measurements, we found that the reactivity trend of the PdAu/N_xC in the ECRR can be intrinsically correlated with work function of the catalysts. PdAu/$N_{7.50}$C with the highest N contents displays a 100% CO_2-to-CO conversion and high conversion efficiency over a wide potential window, superior over other reported PdAu catalysts. This work provides a new way to boost ECRR by lowering the work function of the metal/carbon electrocatalysts.

2. Results and discussion

The synthesis procedure of PdAu/N_xC is illustrated in Fig. 1a. Polymer precursor containing Pd source was first synthesized by a hydrothermal process using 3-aminophenol (3-AP) as both N and C source, F127 as template, and K_2PdCl_4 as Pd source. Subsequently, Au precursor, $[AuCl_4]^-$, was introduced into the polymer precursor by weak coordination between N-containing functional groups in polymer and Au ions. As a result, N-rich polymer precursor containing bimetallic ion source was formed. Finally, PdAu/N_xC dyads composed of PdAu bimetallic NPs and N-doped carbon supports were obtained after pyrolysis and ozone-air flow treatment. The N content of the above sample was 5.4 at% (Fig. S1 and Table S1). Additionally, the N contents could be increased from 5.4 at% to 7.1 and 7.5 at% by adding different amounts of dicyanodiamine (DCD) as additional N source, and decreased from 5.4 at% to 5.2 at% by replacing 3-AP with N-free resorcinol (Table S2 and Fig. S2). The obtained samples were denoted as PdAu/N_xC, where x refers to the atomic ratio of N in the PdAu/N_xC dyads. In addition, PdAu nanoparticles supported on N-free carbon black (PdAu/C) sample, metal-free N-doped carbon (NC), and Au nanoparticles supported on N-doped carbon (Au/N_xC) were also prepared for reference (Figs. S3 and S4). The tunable N content enables a possible way to associate the catalytic activity with work function of electrocatalysts and will be discussed in detail below.

Scanning electron microscope (SEM) images show that the samples have a three-dimensional coral-like structure (Fig. S5). Transmission electron microscopy (TEM) discloses that ultrafine metallic NPs with a narrow size distribution (~5.7 nm) are homogeneously dispersed on porous carbon support (Fig. 1b). Further high-resolution TEM studies reveal the formation of a highly coupled interface of metals and graphitic carbon layers (Fig. 1c). We also used high-angle annular dark-field scanning transmission electron microscopy (HAADF-STEM) for revealing the state of metal species. As shown in Fig. 1d, the bright dots are well dispersed metallic NPs. Energy-dispersive X-ray spectroscopy (EDX) mapping images imply that the distributions of Pd and Au almost overlap with each other, indicating the formation of PdAu bimetallic NPs (Figs. 1e-1h). X-ray diffraction (XRD) patterns further indicate that Pd is incorporated into the Au structure to form an alloy phase (Fig. S6). A homogeneous distribution of N atoms along the whole carbon support indicates an integrated structure of PdAu NPs on the N-doped carbons. Based on inductively coupled plasma-optical emission spectrometer

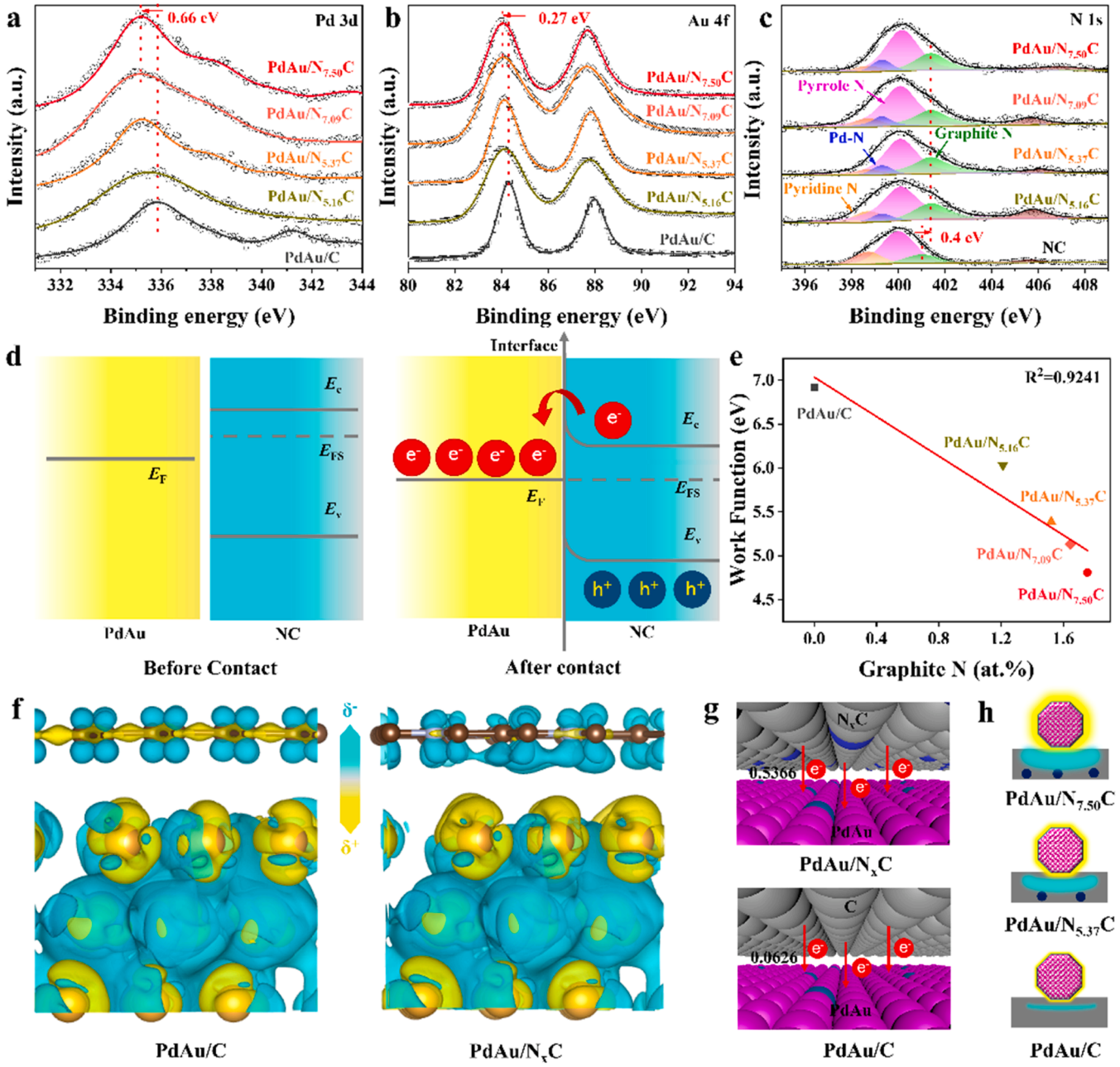

Fig. 2. XPS spectra of Pd 3d (a) and Au 4 f (b) of PdAu/N_xC and PdAu/C, (c) XPS spectra of N1s of PdAu/N_xC and NC, (d) schematic illustration of the PdAu and NC before and after contact, (e) the correlation of work function with the content of graphite N, (f) differential charge density redistributions in PdAu/N_xC and PdAu/C, (g) schematic diagram for the charge transfer between PdAu and NC, (h) schematic diagram for electron density of PdAu/N_xC.

(ICP-OES) analysis, the amount of Pd and Au in PdAu/$N_{7.50}$C are 0.11 wt % and 4.7 wt%, respectively, and all the samples show similar metal contents (Table S3).

We investigated the electronic interactions between PdAu and carbon support by X-ray photoelectron spectroscopy (XPS) first. As shown in Figs. 2a and 2b, the gradual shifts of typical Pd $3d_{5/2}$ and Au 4 $f_{7/2}$ peaks to lower energy indicate the gradually richer electron density of PdAu in PdAu/N_xC samples with the incorporation of more N dopants. For N 1 s spectra, the energy peak positions of graphitic N in PdAu/N_xC shift to higher energy compared with that in NC, indicating the decrease of the electron density of N in carbon support after bimetallic PdAu decoration (Fig. 2c and Table S4). Those results mean a spontaneous electron donation from the N-rich carbon supports to the PdAu NPs at their coupling interface (Fig. 2d). The flow of electrons is significantly affected by the N content because of the difference of work function of PdAu and N-doped carbon [29]. According to the UPS results (Fig. S7), there is a significant shift of secondary electron cutoff towards lower kinetic energy or a noticeable reduction of the work function of the heterostructures with the incorporation of N dopants. The work functions of PdAu/$N_{7.50}$C, PdAu/$N_{7.09}$C, PdAu/$N_{5.37}$C, PdAu/$N_{5.16}$C and PdAu/C were calculated to be 4.81 eV, 5.13 eV, 5.39 eV, 6.03 eV and 6.92 eV, respectively. Furthermore, the contents of pyrrole N and graphite N show good linear relationships with work function (Fig. 2e and S8), indicating that the latter can be regulated by the former [30].

The behavior of electron transfer between PdAu and carbon was further theoretically elucidated by Bader charge analysis. The electron density difference stereograms of PdAu/N_xC model in Fig. 2f illustrate the significant electron transfer from N atoms in NC to PdAu, resulting in more pronounced electron-rich regions in PdAu NPs compared to the same PdAu model supported on pristine carbon (PdAu/C). The total

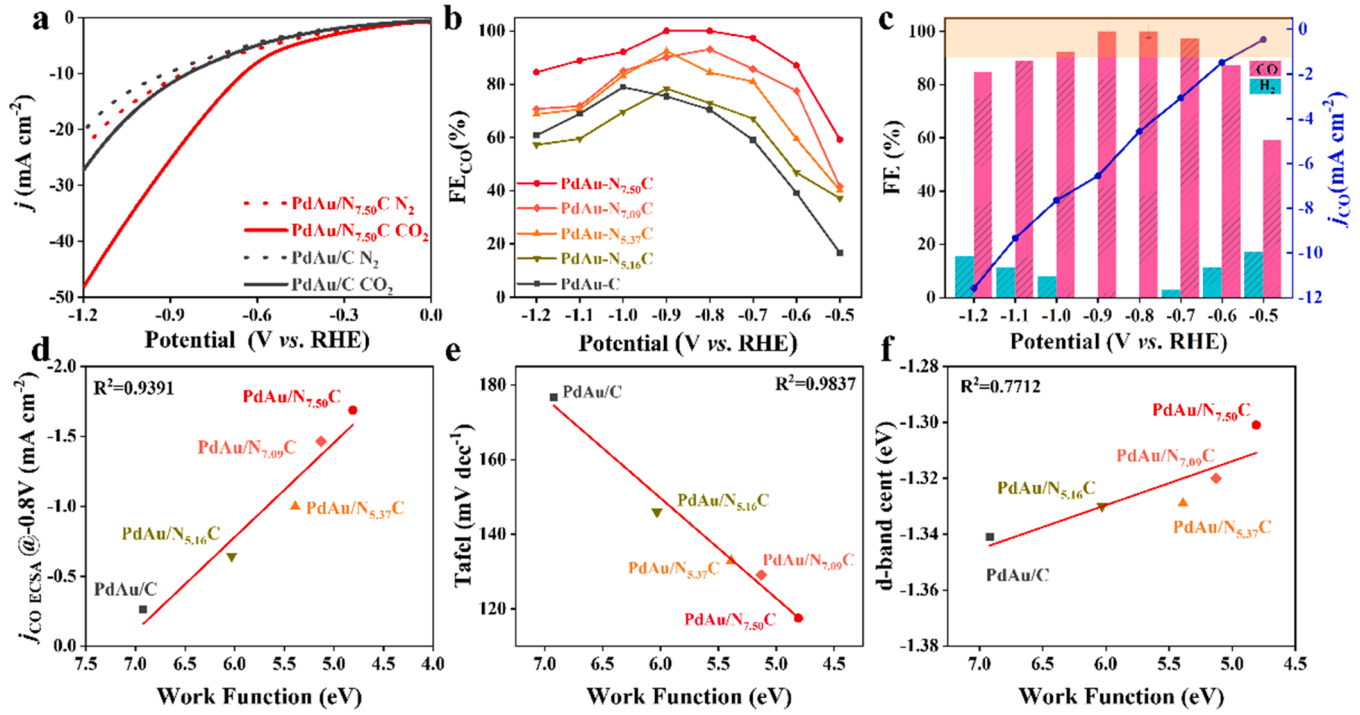

Fig. 3. (a) Linear sweep voltammetry (LSV) curves of PdAu/$N_{7.50}$C and PdAu/C in CO_2- or N_2-saturated 0.1 M $KHCO_3$ solution, (b) FE_{CO} of PdAu/N_xC and PdAu/C at various potentials, (c) FE_{CO} and CO partial current density of PdAu/$N_{7.50}$C, (d) correlation of $j_{CO\ ECSA}$ at − 0.8 V with work functions, (e) correlation of Tafel slope with work functions, (f) correlation of D-band center and work function.

number of electrons transferred from NC support to the ultrafine PdAu nanoparticles is 0.5366 eV, significantly higher than that for carbon without N dopant (0.0626 eV) (Fig. 2g). All of the above results indicate the formation of electron-rich PdAu NPs and the possibility to further enhance the electron density by increasing the N contents in the carbon supports (Fig. 2h), which provides a platform to construct correlation of ECRR performance and work function of electrocatalysts.

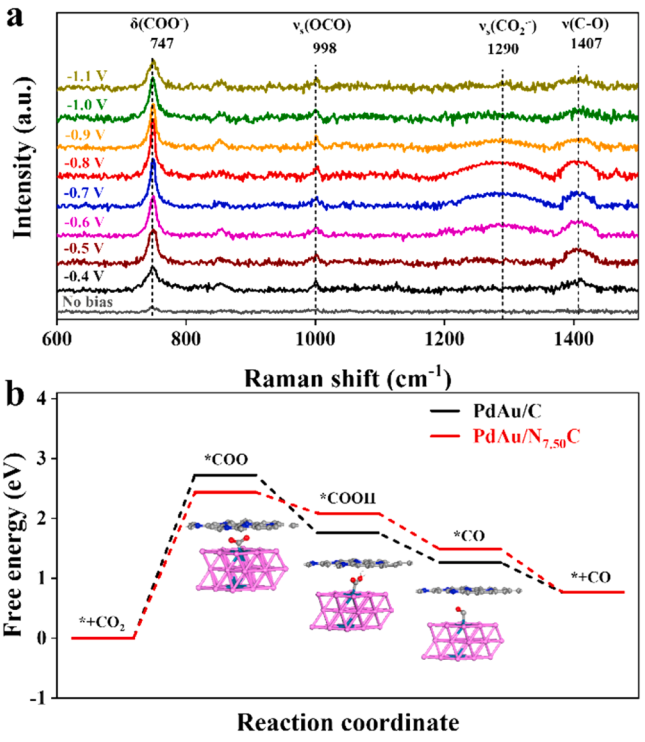

Fig. 4. (a) The electrochemical in-situ surface enhanced Raman spectroscopy of PdAu/$N_{7.50}$C in 0.1 M CO_2-saturated $KHCO_3$, (b) the Gibbs free energy diagrams for ECRR on PdAu/$N_{7.50}$C and PdAu/C.

Inspired by the success in modifying the electron density of the ultrafine PdAu NPs, we further evaluated the catalytic activity of PdAu/N_xC and PdAu/C catalysts for ECRR in an H-cell containing CO_2- or N_2-saturated 0.1 M $KHCO_3$ electrolyte. Compared with N_2-saturated electrolyte, the linear sweep voltammetry (LSV) curves in CO_2-saturated electrolyte for the PdAu/N_xC and PdAu/C catalysts all showed sharp reduction peaks, suggesting that CO_2 can be activated on all the catalysts (Fig. 3a and S9). At the measured potential range, N-containing samples showed significantly higher catalytic currents than that of PdAu/C samples with the order of PdAu/$N_{7.50}$C > PdAu/$N_{7.09}$C > PdAu/$N_{5.37}$C > PdAu/$N_{5.16}$C > PdAu/C. Quantified by gas and ion chromatography, the products in CO_2 electroreduction are CO and H_2 over all the catalysts. Remarkably, PdAu/$N_{7.50}$C exhibits the highest FE_{CO} in all potential range compared with those for PdAu/$N_{7.09}$C, PdAu/$N_{5.37}$C, PdAu/$N_{5.16}$C and PdAu/C (Fig. 3b and S10). As shown in Fig. 3c, PdAu/$N_{7.50}$C shows 100% CO selectivity at − 0.8 V to − 0.9 V vs. RHE and FE_{CO} steadily preserves more than 90% over a wide potential range from − 0.7 V to − 1.0 V. The ECRR selectivity and operation potential range for high FE_{CO} are superior over the most advanced PdAu bimetallic ECRR electrocatalysts in the H-type cell (Table S5).

The impressive activity and selectivity result in excellent efficiency of CO formation (Fig. S11 and S12). Taking − 0.8 V as an example, PdAu/$N_{7.50}$C exhibits a CO partial current density normalized by ECSA ($j_{CO\ ECSA}$) of − 1.69 mA cm^{-2}, which is 6.5 times that of PdAu/C (−0.26 mA cm^{-2}) and higher than other N-doped samples. Notably, a linear relationship was clearly observed by plotting those $j_{CO\ ECSA}$ vs. the work function of corresponding electrocatalysts (Fig. 3d), indicating that the decrease of work function leads to an enhanced electroconversion of CO_2-to-CO activity. The effect of work function on the kinetic perspective of ECRR was evaluated by Tafel analysis. The Tafel slope tends to decrease with the decrease of work function, illustrating a kinetics enhancement behavior (Figs. S13).[31] Moreover, the

correlation of the Tafel slope for the as-prepared samples with their work functions shows the same trends as activity (Fig. 3e), confirming that the work function can be an effective descriptor for the ECRR activity and reaction kinetics. This suggests that an electrocatalyst with lower work function is favorable for donating electron from the electrocatalyst surface to the adsorbed intermediates, thereby boosting the performance of PdAu/N_xC in ECRR. To the best of our knowledge, the application of the work function as ECRR reaction activity and kinetics descriptor is not reported before. In addition, the work function and the D-band center are linearly proportional (Fig. 3f, Table S6 and Fig. S14). This means that the D-band center of metal also can be used to describe the activity of catalysts. Notably, the catalytic performance and the work function of Au/N_xC are also correlated (Fig. S15-S18), which further illustrates the high applicability of the work function as the ECRR reactivity descriptor.

To evaluate the long-term stability, we tested the PdAu/$N_{7.50}$C and PdAu/C under the same ECRR conditions. The total current density of PdAu/$N_{7.50}$C was stable during the stability test and FE_{CO} is maintained at more than 90% in consecutive operation of 12 h (Fig. S19). In contrast, the FE_{CO} on PdAu/C degraded quickly from 75% to 53% after 12 h operation. After the long-term testing, the morphology and chemical structure of PdAu/$N_{7.50}$C were well-preserved (Figs. S20 and S21). In contrast, the original small nanoparticles (~6.8 nm) of PdAu/C severely aggregated into around 14.6 nm (Fig. S22). The remarkably enhanced ECRR stability of PdAu/$N_{7.50}$C can be attributed to the effective prevention of PdAu NPs from aggregation benefitting from the confinement effect and interfacial engineering.[32].

To obtain the essential understanding of ECRR mechanism, we used the electrochemical in-situ surface enhanced Raman spectroscopy (SERS) to observe the conceivable reaction intermediates at various potentials (Fig. 4a). Four peaks (747, 998, 1290 and 1407 cm^{-1}) were observed from − 0.4 V to − 1.0 V, which can be allocated to the bending vibration of *COO^-, the *OCO symmetrical stretching for *COOH, the C═O stretching vibration of surface-adsorbed carbonate $\nu_s(CO_2^-)$ and the C-O stretching vibration of *COOH, respectively. [33–35] As the potential increases from − 0.4 V to − 1.0 V, the signal goes from weak to strong and then to weak. When voltages higher than − 1.0 V were applied, the reaction rate increased due to the relatively large driving force, enabling a speedy depletion of the intermediate, resulting in weak signals.[36].

To get insights into the effect of N doping of PdAu/N_xC on the ECRR mechanism, we constructed the models of PdAu/$N_{7.50}$C and PdAu/C with adsorption of the intermediates based on the in-situ SERS and performed the DFT calculations. Specifically, the free energy profiles for ECRR to CO on PdAu/$N_{7.50}$C and PdAu/C were calculated including CO_2 adsorption, *COOH formation, *CO formation, and CO desorption (Fig. 4b). For both PdAu/N_xC and PdAu/C, the formation of the *COO^- intermediate has the highest energy barrier, indicating that this is the rate-limiting step. Then, we calculated the rate-determining barrier of PdAu/N_xC electrocatalytic reduction of CO_2 (Fig. S23). Interestingly, the free energy required for the formation of *COO^- intermediate by PdAu/N_xC is obviously lower than that of PdAu/C, confirming that the increased interface potential is more conducive to the adsorption of *COO^- intermediates.

3. Conclusion

In summary, a series of highly coupled PdAu/N-rich carbon dyads were successfully synthesized by precise control of N contents for modulating the electron density of PdAu bimetallic NPs. Spontaneous electron transfer from carbon to PdAu was confirmed by both experimental and theoretical analysis. Increasing the N content of carbon significantly reduced work function of the catalysts. As a result, donating electrons from the catalyst surface to the adsorbed intermediates (*COO^-) was facilitated, thereby boosting the performance of PdAu/N_xC in ECRR. PdAu/$N_{7.50}$C catalyst achieves a 100% CO_2-to-CO conversion and high conversion efficiency over a wide potential window, superior over other reported PdAu catalysts. More importantly, the linear relationships of the work function with activity and reaction kinetics were established, enabling the application of the work function as a descriptor for ECRR reaction activity and kinetics. The procedure is simple and reproducible, providing a general design principle for enhancing the activity in other electrochemical reactions.

CRediT authorship contribution statement

The manuscript was written through contributions of all authors. All authors have given approval to the final version of the manuscript.

Declaration of Competing Interest

The authors declare that they have no known competing financial interests or personal relationships that could have appeared to influence the work reported in this paper.

Data Availability

Data will be made available on request.

Acknowledgements

This paper is dedicated to the 120th anniversary of Hebei University of Technology. This work was supported by the National Natural Science Foundation of China (No. 22008048 and 22278108), Hundred Talents Project of Hebei Province (No. E2019050015), Joint Funds of the National Natural Science Foundation of China (U20A20302), Innovative Group Projects in Hebei Province (E2021202006), Natural Science Foundation for Outstanding Youth Scholars of Hebei Province (No. B2021202061), Natural Science Foundation of Tianjin (22JCYBJC00250), Natural Science Foundation of Hebei Province (No. B2021202010), the State Key Laboratory of Fine Chemicals, Dalian University of Technology (KF 2108), Open Research Fund of CNMGE Platform & NSCC-TJ (CNMGE2022006), and Bianshui Riverside Supercomputing Center (BRSC).

Appendix A. Supplementary material

Supporting Information contains this information is available free of charge via the Internet.

Appendix A. Supporting information

Supplementary data associated with this article can be found in the online version at doi:10.1016/j.apcatb.2023.122931.

References

[1] X. Tan, C. Yu, Y. Ren, S. Cui, W. Li, J. Qiu, Recent advances in innovative strategies for the CO_2 electroreduction reaction, Energy Environ. Sci. 14 (2021) 765–780, https://doi.org/10.1039/d0ee02981e.

[2] D. Chen, L.H. Zhang, J. Du, H. Wang, J. Guo, J. Zhan, F. Li, F. Yu, A. Tandem, Strategy for enhancing electrochemical CO_2 reduction activity of single-atom Cu-S_1N_3 catalysts via integration with Cu nanoclusters, Angew. Chem. Int. Ed. 60 (2021) 24022–24027, https://doi.org/10.1002/anie.202109579.

[3] Z. Cai, N. Cao, F. Zhang, X. Lv, K. Wang, Y. He, Y. Shi, H. Bin Wu, P. Xie, Hierarchical Ag-Cu interfaces promote C-C coupling in tandem CO_2 electroreduction, Appl. Catal. B Environ. 325 (2023), 122310, https://doi.org/10.1016/j.apcatb.2022.122310.

[4] W. Xiong, D. Si, J. Yi, Y. Huang, H. Li, R. Cao, Morphology and composition dependence of multicomponent Cu-based nanoreactor for tandem electrocatalysis CO_2 reduction, Appl. Catal. B Environ. 314 (2022), 121498, https://doi.org/10.1016/j.apcatb.2022.121498.

[5] D. Gao, H. Zhou, J. Wang, S. Miao, F. Yang, G. Wang, J. Wang, X. Bao, Size-dependent electrocatalytic reduction of CO_2 over Pd nanoparticles, J. Am. Chem. Soc. 137 (2015) 4288–4291, https://doi.org/10.1021/jacs.5b00046.

[6] Z. Li, D. He, X. Yan, S. Dai, S. Younan, Z. Ke, X. Pan, X. Xiao, H. Wu, J. Gu, Size-dependent nickel-based electrocatalysts for selective CO_2 reduction, Angew. Chem. Int. Ed. 59 (2020) 18572–18577, https://doi.org/10.1002/anie.202000318.
[7] X. Deng, D. Alfonso, T.-D. Nguyen-Phan, D.R. Kauffman, Resolving the size-dependent transition between CO_2 reduction reaction and H_2 evolution reaction selectivity in Sub-5 nm silver nanoparticle electrocatalysts, ACS Catal. (2022) 5921–5929, https://doi.org/10.1021/acscatal.2c00960.
[8] W. Rong, H. Zou, W. Zang, S. Xi, S. Wei, B. Long, J. Hu, Y. Ji, L. Duan, Size-dependent activity and selectivity of atomic-level copper nanoclusters during CO/CO_2 electroreduction, Angew. Chem. Int. Ed. 60 (2021) 466–472, https://doi.org/10.1002/anie.202011836.
[9] C. Gao, F. Lyu, Y. Yin, Encapsulated metal nanoparticles for catalysis, Chem. Rev. 121 (2021) 834–881, https://doi.org/10.1021/acs.chemrev.0c00237.
[10] J.M. Yoo, H. Shin, D.Y. Chung, Y.E. Sung, Carbon shell on active nanocatalyst for stable electrocatalysis, Acc. Chem. Res. 55 (2022) 1278–1289, https://doi.org/10.1021/acs.accounts.1c00727.
[11] W. Zhang, S. Bu, Q. Yuan, Q. Xu, M. Hu, Controllable nitrogen-doping of nanoporous carbons enabled by coordination frameworks, J. Mater. Chem. A 7 (2019) 647–656, https://doi.org/10.1039/c8ta09817d.
[12] G.-H. Wang, K. Chen, J. Engelhardt, H. Tüysüz, H.-J. Bongard, W. Schmidt, F. Schüth, Scalable one-pot synthesis of yolk−shell carbon nanospheres with yolk-supported Pd nanoparticles for size-selective catalysis, Chem. Mater. 30 (2018) 2483–2487, https://doi.org/10.1021/acs.chemmater.8b00456.
[13] C. Yan, W. Luo, H. Yuan, G. Liu, R. Hao, N. Qin, Z. Wang, K. Liu, Z. Wang, D. Cui, Z. Hu, Y. Lan, Z. Lu, Stabilizing intermediates and optimizing reaction processes with N doping in Cu_2O for enhanced CO_2 electroreduction, Appl. Catal. B Environ. 308 (2022), 121191, https://doi.org/10.1016/j.apcatb.2022.121191.
[14] P. Blonski, J. Tucek, Z. Sofer, V. Mazanek, M. Petr, M. Pumera, M. Otyepka, R. Zboril, Doping with graphitic nitrogen triggers ferromagnetism in graphene, J. Am. Chem. Soc. 139 (2017) 3171–3180, https://doi.org/10.1021/jacs.6b12934.
[15] Z. Jin, J. Yao, C. Kittre, J.M. Tour, Large-scale growth and characterizations of nitrogen-doped monolayer graphene sheets, ACS Nano 5 (2011) 4112–4117, https://doi.org/10.1021/nn200766e.
[16] X. Wang, X. Li, L. Zhang, Y. Yoon, P.K. Weber, H. Wang, J. Guo, H. Dai, N-doping of graphene through electrothermal reactions with ammonia, Science 324 (2009), https://doi.org/10.1126/science.1170335, 768-711.
[17] J.Y. Cheon, J.H. Kim, J.H. Kim, K.C. Goddeti, J.Y. Park, S.H. Joo, Intrinsic relationship between enhanced oxygen reduction reaction activity and nanoscale work function of doped carbons, J. Am. Chem. Soc. 136 (2014) 8875–8878, https://doi.org/10.1021/ja503557x.
[18] M.D. Rötzer, M. Krause, A.S. Crampton, U. Heiz, B. Yoon, U. Landman, Nanotuning via local work function control: ethylene hydrogenation on supported Pt nanoclusters, ACS Catal. 10 (2019) 1799–1809, https://doi.org/10.1021/acscatal.9b03890.
[19] M. Yuan, Y. Bai, J. Zhang, T. Zhao, S. Li, H. He, Z. Liu, Z. Wang, G. Zhang, Work function regulation of nitrogen-doped carbon nanotubes triggered by metal nanoparticles for efficient electrocatalytic nitrogen fixation, J. Mater. Chem. A 8 (2020) 26066–26074, https://doi.org/10.1039/d0ta08914a.
[20] H. Liu, J. Guan, S. Yang, Y. Yu, R. Shao, Z. Zhang, M. Dou, F. Wang, Q. Xu, Metal-organic-framework-derived Co_2P nanoparticle/multi-doped porous carbon as a trifunctional electrocatalyst, Adv. Mater. 32 (2020), e2003649, https://doi.org/10.1002/adma.202003649.
[21] P. Su, W. Pei, X. Wang, Y. Ma, Q. Jiang, J. Liang, S. Zhou, J. Zhao, J. Liu, G.Q. M. Lu, Exceptional electrochemical HER performance with enhanced electron transfer between Ru nanoparticles and single atoms dispersed on a carbon substrate, Angew. Chem. Int. Ed. 60 (2021) 16044–16050, https://doi.org/10.1002/anie.202103557.
[22] W.J. Sun, H.Q. Ji, L.X. Li, H.Y. Zhang, Z.K. Wang, J.H. He, J.M. Lu, Built-in electric field triggered interfacial accumulation effect for efficient nitrate removal at ultra-low concentration and electroreduction to ammonia, Angew. Chem. Int. Ed. 60 (2021) 22933–22939, https://doi.org/10.1002/anie.202109785.
[23] W. Zhang, E.J. Meeus, L. Wang, L.H. Zhang, S. Yang, B. de Bruin, J.N.H. Reek, F. Yu, Boosting electrochemical oxygen reduction performance of iron phthalocyanine through axial coordination sphere interaction, ChemSusChem 15 (2022), e202102379, https://doi.org/10.1002/cssc.202102379.
[24] X. Fan, S. Zerebecki, R. Du, R. Hubner, G. Marzum, G. Jiang, Y. Hu, S. Barcikowki, S. Reichenberger, A. Eychmuller, Promoting the electrocatalytic performance of noble metal aerogels by ligand-directed modulation, Angew. Chem. Int. Ed. 59 (2020) 5706–5711, https://doi.org/10.1002/anie.201913079.
[25] P. Gao, Z.H. Xue, S.N. Zhang, D. Xu, G.Y. Zhai, Q.Y. Li, J.S. Chen, X.H. Li, Schottky barrier-induced surface electric field boosts universal reduction of NO_x^- in water to ammonia, Angew. Chem. Int. Ed. 60 (2021) 20711–20716, https://doi.org/10.1002/anie.202107858.
[26] Y.X. Liu, H.H. Wang, T.J. Zhao, B. Zhang, H. Su, Z.H. Xue, X.H. Li, J.S. Chen, Schottky barrier induced coupled interface of electron-rich N-doped carbon and electron-deficient Cu: in-built lewis acid-base pairs for highly efficient CO_2 fixation, J. Am. Chem. Soc. 141 (2019) 38–41, https://doi.org/10.1021/jacs.8b08267.
[27] Y. Kim, G. Collinge, M.S. Lee, K. Khivantsev, S.J. Cho, V.A. Glezakou, R. Rousseau, J. Szanyi, J.H. Kwak, Surface density dependent catalytic activity of single palladium atoms supported on ceria, Angew. Chem. Int. Ed. 60 (2021) 22769–22775, https://doi.org/10.1002/anie.202105750.
[28] Z. Nie, L. Zhang, X. Ding, M. Cong, F. Xu, L. Ma, M. Guo, M. Li, L. Zhang, Catalytic kinetics regulation for enhanced electrochemical nitrogen oxidation by ru-nanoclusters-coupled Mn_3O_4 catalysts decorated with atomically dispersed ru atoms, Adv. Mater. 34 (2022) 2108180, https://doi.org/10.1002/adma.202108180.
[29] Z. Wang, X. Zhuang, B. Wang, W. Huang, T.J. Marks, A. Facchetti, Doping indium oxide films with amino-polymers of varying nitrogen content markedly affects charge transport and mechanical flexibility, Adv. Funct. Mater. 31 (2021) 2100451, https://doi.org/10.1002/adfm.202100451.
[30] K. Yokoyama, Y. Sato, M. Yamamoto, T. Nishida, K. Motomiya, K. Tohji, Y. Sato, Work function, carrier type, and conductivity of nitrogen-doped single-walled carbon nanotube catalysts prepared by annealing via defluorination and efficient oxygen reduction reaction, Carbon 142 (2019) 518–527, https://doi.org/10.1016/j.carbon.2018.10.052.
[31] Y. Wang, Y. Li, J. Liu, C. Dong, C. Xiao, L. Cheng, H. Jiang, H. Jiang, C. Li, $BiPO_4$-derived 2D nanosheets for efficient electrocatalytic reduction of CO_2 to liquid, Fuel, Angew. Chem. Int. Ed. 60 (2021) 7681–7685, https://doi.org/10.1002/anie.202014341.
[32] T. Zhou, H. Shan, H. Yu, C. Zhong, J. Ge, N. Zhang, W. Chu, W. Yan, Q. Xu, H. Wu, C. Wu, Y. Xie, Nanopore confinement of electrocatalysts optimizing triple transport for an ultrahigh-power-density zinc-air fuel cell with robust stability, Adv. Mater. 32 (2020), e2003251, https://doi.org/10.1002/adma.202003251.
[33] W. Shan, R. Liu, H. Zhao, Z. He, Y. Lai, S. Li, G. He, J. Liu, In situ surface-enhanced raman spectroscopic evidence on the origin of selectivity in CO_2 electrocatalytic reduction, ACS Nano 14 (2020) 11363–11372, https://doi.org/10.1021/acsnano.0c03534.
[34] G.-Y. Duan, X.-Q. Li, Y.-R. Du, B.-H. Xu, Efficient electrocatalytic reduction of CO_2 to CO on highly dispersed Ag nanoparticles confined by Poly(ionic liquid, Chem. Eng. J. 455 (2023), 140910, https://doi.org/10.1016/j.cej.2022.140910.
[35] J. Duan, T. Liu, Y. Zhao, R. Yang, Y. Zhao, W. Wang, Y. Liu, H. Li, Y. Li, T. Zhai, Active and conductive layer stacked superlattices for highly selective CO_2 electroreduction, Nat. Commun. 13 (2022) 2039, https://doi.org/10.1038/s41467-022-29699-2.
[36] J. Guo, W. Zhang, L.H. Zhang, D. Chen, J. Zhan, X. Wang, N.R. Shiju, F. Yu, Control over electrochemical CO_2 reduction selectivity by coordination engineering of tin single-atom catalysts, Adv. Sci. 8 (2021), e2102884, https://doi.org/10.1002/advs.202102884.